Week 8
Lecture Notes:
Topological Condensed Matter Physics

Sebastian Huber and Titus Neupert

Department of Physics, ETH Zürich
Department of Physics, University of Zürich

If you notice mistakes or typos, please report them to michael.denner@physik.uzh.ch or periv@phys.ethz.ch

Chapter 8

Topological Crystalline Insulators I

Learning goals

- We understand how the topological classification of insulators and the bulk-boundary correspondence is enhanced by including crystalline symmetries.
- We know how topological invariants such as mirror-graded winding numbers and the mirror Chern number are defined.
- We have an understanding of higher-order topological insulators.

- L. Fu, Phys. Rev. Lett. **106**, 106802 (2011)
- C. Fang and L. Fu, Phys. Rev. B. **91**, 161105 (2015)
- W. Benalcazar, B. A. Bernevig, Science **357**, 61–66 (2017)
- W. Benalcazar, F. Schindler *et al.*, Science Adv. **4**, eaat0346 (2018)

Topological crystalline insulators are protected by spatial symmetry transformations which act non-locally such as mirror or rotational symmetries. They are usually identified with two notions: i) their bulk ground state is not adiabatically connected to an atomic limit without breaking the protecting symmetry. ii) they have gapless boundary modes which can only be gapped out by breaking the respective symmetry.
In fact, properties i) and ii) are not equivalent. We have already seen for the case of the SSH model protected by inversion symmetry that it is possible to have a model featuring i) but not ii). [1] The reason was that although the model in its topological phase (as detectable by, e.g., the Wilson loop) is not adiabatically connected to any atomic limit, there is no boundary which is left invariant by inversion symmetry, and thus no protected edge modes (as long as we do not consider chiral symmetry, which is local and therefore non-crystalline). This is a general feature of topological crystalline insulators: gapless symmetry-protected boundary modes also require the boundary on which they are localized to preserve the corresponding symmetry. In the following, we discuss several examples of topological crystalline phases and their invariants.

8.1 2D topological crystalline insulator

Here we show how crystalline symmetries can enrich the topological classification of band structures. We begin with a model with chiral symmetry in 2D. A natural non-local symmetry in 2D

[1] To be more precise, we have to differentiate more carefully: The two inversion-symmetry protected phases of the SSH model are actually both atomic limits, in the sense that the ground state can be written as a single Slater determinant of exponentially localized Wannier functions. However, these two atomic limits differ in the location (Wyckoff position) on which the Wannier function is localized. Therefore these two atomic limits are not adiabatically connected. More details on that point of view will follow in the lecture on topological quantum chemistry.

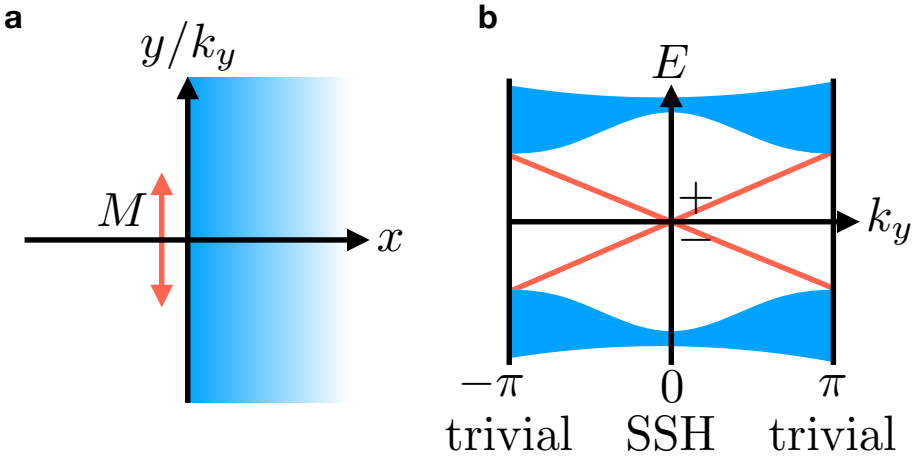

Figure 8.1: Real space geometry and spectrum of the mirror symmetric 2D model of a chiral symmetric topological crystalline insulator. ***a*** We consider a geometry where the system is terminated in x-direction but periodic in y-direction, retaining k_y as momentum quantum number. In particular, note that the surface in this semi-infinite slab geometry is mapped onto itself by the $M = M_y$ mirror symmetry, and therefore hosts gapless modes stemming from the nontrivial topology of the bulk. ***b*** Schematic spectrum of the model given by Eq. (8.1.1) in the presence of the bulk termination in x-direction. There are two counter-propagating chiral modes which are necessarily crossing at $k_y = 0$ due to the chiral symmetry. At hat point, they are also eigenstates of the mirror symmetry with eigenvalue ± 1, respectively. They are therefore protected from hybridization by the mirror symmetry.

we can add is a mirror symmetry, which leaves an edge invariant. While all 2D systems with just chiral symmetry (class AIII in the tenfold way) are topologically trivial, it will turn out that with mirror symmetry this is no longer the case when we require that mirror and chiral symmetry transformations commute.
The model we consider here is defined by the Bloch Hamiltonian

$$\begin{aligned} \mathcal{H}(\boldsymbol{k}) &= \begin{pmatrix} 0 & q(\boldsymbol{k}) \\ q^\dagger(\boldsymbol{k}) & 0 \end{pmatrix}, \\ q(\boldsymbol{k}) &= \begin{pmatrix} (1-\cos k_y) + e^{\mathrm{i}k_x} + \lambda & \sin k_y \\ -\sin k_y & (1-\cos k_y) + e^{-\mathrm{i}k_x} - \lambda \end{pmatrix}. \end{aligned} \tag{8.1.1}$$

The symmetry representations are

$$\begin{aligned} C\mathcal{H}(\boldsymbol{k})C^{-1} &= -\mathcal{H}(\boldsymbol{k}), \quad M_y\mathcal{H}(k_x,k_y)M_y^{-1} = \mathcal{H}(k_x,-k_y), \\ C &= \begin{pmatrix} \mathbb{1}_{2\times 2} & 0 \\ 0 & -\mathbb{1}_{2\times 2} \end{pmatrix}, \quad M_y = \begin{pmatrix} \sigma_z & 0 \\ 0 & \sigma_z \end{pmatrix}, \end{aligned} \tag{8.1.2}$$

where $\mathbb{1}_{2\times 2}$ denotes the 2×2 identity matrix and λ represents a numerically small perturbation that breaks M_x symmetry. When we calculate the winding number along the path $k_x = 0 \to k_x = 2\pi$, $k_y = $ const. in the BZ, we find $\nu(k_y) = 0\ \forall k_y$. We can most easily see this by evaluating $\nu(0) = 0$ and noting that as the spectrum is gapped throughout the BZ, and the model has chiral symmetry, the result holds for all k_y.
In the presence of mirror symmetry, however, we can refine the topological characterization. Since in our case mirror symmetry satisfies $M_y^2 = 1$, its representation has eigenvalues ± 1. Given any line l_{M_y} in the BZ which is left invariant under the action of M_y, the eigenstates $|u_{\boldsymbol{k},n}\rangle$ of

$\mathcal{H}$ on l_{M_y} can be decomposed into two groups, $\{|u^+_{\boldsymbol{k},l}\rangle\}$ and $\{|u^-_{\boldsymbol{k},l'}\rangle\}$, with mirror eigenvalue ± 1, respectively. We can define the Wilson loop in each mirror subspace as

$$W^{\pm}[l_{M_y}] = \overline{\exp}\left[-\int_{l_{M_y}} \mathrm{d}\boldsymbol{l}_{\boldsymbol{M_y}} \cdot \boldsymbol{\mathcal{A}}^{\pm}(\boldsymbol{k})\right], \tag{8.1.3}$$

where we have used the mirror-graded Berry connection

$$\boldsymbol{\mathcal{A}}^{\pm}_{m,n}(\boldsymbol{k}) = \langle u^{\pm}_{\boldsymbol{k},m}|\boldsymbol{\nabla}_{\boldsymbol{k}}|u^{\pm}_{\boldsymbol{k},n}\rangle, \qquad n,m = 1,\cdots,M. \tag{8.1.4}$$

For the two mirror invariant paths $l_{M_y} : k_x = 0 \to k_x = 2\pi, k_y = 0, \pi$, the mirror-graded topological polarization invariants evaluate to

$$\mathsf{P}_{M_y}(k_y) = \frac{1}{2}\left[\left(-\frac{\mathrm{i}}{2\pi}\log W^+(k_y)\right) - \left(-\frac{\mathrm{i}}{2\pi}\log W^-(k_y)\right)\right] = \begin{cases} 1/2 & k_y = 0 \\ 0 & k_y = \pi \end{cases}, \tag{8.1.5}$$

as can be directly seen from the relation of the model to two mirror-graded copies of the SSH model in the trivial ($k_y = \pi$) and nontrivial ($k_y = 0$) phase. This confirms that the 2D model is in a topologically nontrivial phase protected by mirror and chiral symmetry. With open boundary conditions, we will therefore find gapless states on both edges with normal to the x-direction (see Fig. 8.1***a*** for such a geometry), because these are mapped onto themselves under M_y. Since the model corresponds to a topological-to-trivial tuning of two copies of the SSH model with opposite winding number, we expect two anti-propagating chiral edge states, which cannot gap out at their crossing at $k_y = 0$ since they belong to different mirror subspaces at this point (see Fig. 8.1***b***). A simple way to see this is that mirror symmetry maps $k_y \to -k_y$, while it does not change the energy E. Therefore it exchanges states pairwise at generic momenta k_y and $-k_y$ and we can form symmetric and anti-symmetric superpositions of them to get mirror eigenstates with eigenvalue $+1$ and -1, respectively. The trace of the representation of M_y on this two-dimensional subspace is therefore 0 at almost all momenta and in particular cannot change discontinuously at $k_y = 0$. Alternatively, direct inspection of the Hamiltonian (8.1.1) at $k_y = 0$ reveals that it is composed of two copies of the SSH model, and in view of the form of the mirror symmetry M_y, the two copies reside in opposite mirror subspaces. As a consequence, their end states (the edge modes at $k_y = 0$) also have opposite mirror eigenvalues and cannot hybridize.

Another 2D system which has two anti-propagating chiral edge modes is the quantum spin Hall effect protected by time-reversal symmetry, where the edge modes are localized on all boundaries. It corresponds to two Chern insulators, one for spin up and one for spin down. The present model may be viewed as a close relative, where the edge modes are protected by mirror and chiral symmetry as opposed to time-reversal, and are only present on edges preserving the mirror symmetry.

8.2 Mirror Chern number

In the previous section, we have witnessed an example of a general scheme to construct topological BZ invariants going beyond the tenfold way for systems protected by crystalline symmetries: since a crystalline symmetry acts non-locally in space, it also maps different parts of the BZ onto each other. However, when there are submanifolds of the BZ which are left invariant by the action of the symmetry considered, we may evaluate a non-crystalline invariant on them, suited for the dimension and symmetry class of the corresponding submanifold, as long as we restrict ourselves to one of the symmetry's eigenspaces.

The most prominent example of this construction is the mirror Chern number C_{m} in three-dimensional systems. Since for a spinful system, mirror symmetry M squares to $M^2 = -1$ its

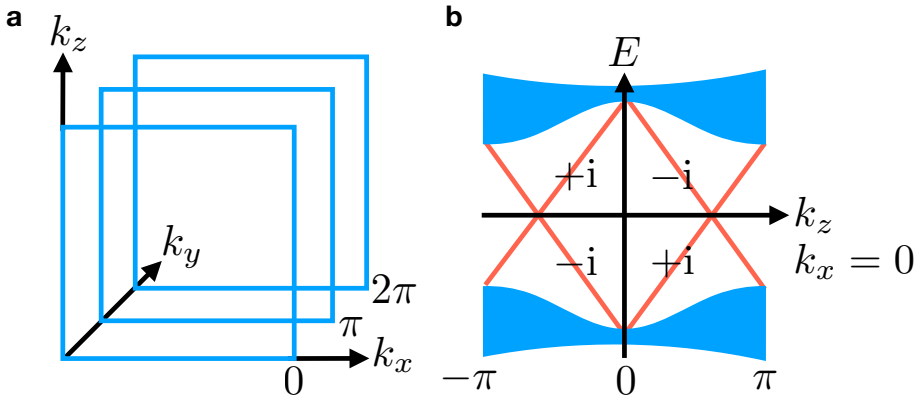

Figure 8.2: Mirror Chern planes in the BZ and schematic surface spectrum for a time-reversal topological crystalline insulator with $C_{\mathrm{m}} = 2$. ***a*** For the mirror symmetry M_y, there are two planes in the BZ which are left invariant by it and can therefore be used to define a mirror Chern number: the plane at $k_y = 0$ and the one at $k_y = \pi$. ***b*** A mirror Chern number $C_{\mathrm{m}} = 2$ enforces the presence of two chiral left-movers and two chiral right-movers along mirror symmetric lines in the surface BZ of any surface mapped onto itself by the mirror symmetry. For M_y, this is, e.g., the case for the surface obtained by terminating the bulk in x-direction and retaining k_y and k_z as momentum quantum numbers. At $k_y = 0$ all bands are eigenstates of the mirror symmetry with eigenvalues as shown, and thus prevented from gapping out. At finite k_y however, hybridization becomes possible and we are left with two Dirac cones in the surface BZ in the case at hand.

representation in this case has eigenvalues $\pm\mathrm{i}$. Let Σ be a surface in the BZ which is left invariant under the action of M, such as the surfaces shown in Fig. 8.2***a*** for M_y. Then, the eigenstates $|u_{\boldsymbol{k},n}\rangle$ of the Hamiltonian on Σ can be decomposed into two groups, $\{|u^{+}_{\boldsymbol{k},l}\rangle\}$ and $\{|u^{-}_{\boldsymbol{k},l'}\rangle\}$, with mirror eigenvalues $+\mathrm{i}$ and $-\mathrm{i}$, respectively. Time-reversal symmetry maps one mirror subspace onto the other; if it is present, the two mirror eigenspaces are of the same dimension. We may define the Chern number in each mirror subspace as

$$C_{\pm} = \frac{1}{2\pi}\int_{\Sigma} dk_x dk_z \mathrm{Tr}\left[\mathcal{F}^{\pm}_{xz}(\boldsymbol{k})\right]. \tag{8.2.1}$$

Here

$$\mathcal{F}^{\pm}_{ab}(\boldsymbol{k}) = \partial_a \mathcal{A}^{+}_{b}(\boldsymbol{k}) - \partial_b \mathcal{A}^{+}_{a}(\boldsymbol{k}) - \mathrm{i}\left[\mathcal{A}^{+}_{a}(\boldsymbol{k}), \mathcal{A}^{+}_{b}(\boldsymbol{k})\right] \tag{8.2.2}$$

is the non-Abelian Berry curvature field in the $\pm\mathrm{i}$ mirror subspace, with $\mathcal{A}^{\pm}_{a;l,l'}(\boldsymbol{k}) = \mathrm{i}\,\langle u^{\pm}_{\boldsymbol{k},l}|\partial_a|u^{\pm}_{\boldsymbol{k},l'}\rangle$, and matrix multiplication is implied. Since $\mathrm{Tr}\left[\mathcal{A}^{+}_{a}(\boldsymbol{k}), \mathcal{A}^{+}_{b}(\boldsymbol{k})\right] = 0$, this corresponds to the usual Chern number, but restricted to a single mirror subspace. Note that in time-reversal symmetric systems we have $C_{+} = -C_{-}$, and can thus define the mirror Chern number

$$C_{\mathrm{m}} := (C_{+} - C_{-})/2. \tag{8.2.3}$$

A non-vanishing mirror Chern number implies that the Bloch Hamiltonian on Σ corresponds to a time-reversal pair of Chern insulators. Thus, the full model will host C_{m} Kramers pairs of gapless modes on an M-invariant line in any surface BZ corresponding to a real space boundary which is mapped onto itself under the mirror symmetry M. These Kramers pairs of modes will be generically gapped out away from the lines in the surface BZ which are invariant under the mirror symmetry, and therefore form surface Dirac cones. Indeed, when C_{m} is odd in a time-reversal symmetric system, this implies an odd number of Dirac cones in any surface BZ, since then the system realizes a conventional time-reversal invariant topological insulator with the

Dirac cones located at time-reversal invariant surface momenta. When C_m is even, the surface Dirac cones exist only on mirror symmetric surfaces and are located at generic momenta along the mirror invariant lines of the surface BZ (see Fig. 8.2***b***). This inherently crystalline case is realized in the band structure of tin telluride, SnTe.

8.3 C_2T-invariant topological crystalline insulator

Here we present another example of a topological crystalline insulator in 3D in order to show that surface Dirac cones protected by crystalline symmetries can also appear at generic, low-symmetry, momenta in the surface BZ. We consider a system that is invariant under the combination C_2T of a two-fold rotation C_2 around the z axis and time-reversal symmetry T. Note that we take both symmetries to be broken individually.
To understand how this symmetry can protect a topological phase, let us review how time-reversal protects a Dirac cone on the surface of a conventional topological insulator. The effective Hamiltonian on the boundary with surface normal along z of a 3D time-reversal symmetric topological insulator takes the form

$$\mathcal{H}(\boldsymbol{k}) = k_y\sigma_x - k_x\sigma_y. \tag{8.3.1}$$

The symmetries are realized as

$$\begin{aligned} T\mathcal{H}(\boldsymbol{k})T^{-1} &= \mathcal{H}(-\boldsymbol{k}), \quad T = \mathrm{i}\sigma_y K, \\ C_2\mathcal{H}(\boldsymbol{k})C_2^{-1} &= \mathcal{H}(-\boldsymbol{k}), \quad C_2 = \sigma_z, \end{aligned} \tag{8.3.2}$$

where we denote by K complex conjugation. Now, the unique mass term for $\mathcal{H}(\boldsymbol{k})$ which gaps out the Dirac cone is $m\sigma_z$. This term is forbidden by time-reversal as expected, since it does not commute with T.
If we dispense with T symmetry and only require invariance under $C_2T = \sigma_x K$, the mass term is still forbidden. However, the addition of other constant terms to the Hamiltonian is now allowed. The freedom we have is to shift the Dirac cone away from the time-reversal symmetric point $\boldsymbol{k} = 0$ by changing the Hamiltonian to

$$\mathcal{H}(\boldsymbol{k}) = (k_y - a)\sigma_x - (k_x - b)\sigma_y, \tag{8.3.3}$$

with some arbitrary parameters a and b. Therefore, the phase stays topologically nontrivial, but has a different boundary spectrum from that of a normal topological insulator. On surfaces preserving C_2^zT symmetry, any odd number of Dirac cones are stable but are in general shifted away from the time-reversal invariant surface momenta. On the surfaces that are not invariant under C_2^zT, the Dirac cones may be gapped out, since T is broken. This amounts to a $\mathbb{Z}_2$ topological classification of C_2^zT-invariant 3D topological crystalline insulators.

8.4 Higher-order topological insulators

So far, when we discussed topological systems in d dimensions, we only considered $(d-1)$ dimensional boundaries which could host gapless states due to the nontrivial topology of the bulk. These systems belong to the class of "first-order" topological insulators. In the following, we will give an introduction to second-order topological insulators which have gapless modes on $(d-2)$ dimensional boundaries, that is, on corners in 2D and hinges in 3D, while the boundaries of dimension $(d-1)$ (i.e., the edges of a 2D system and the surfaces of a 3D system) are generically gapped. Higher-order topological insulators require spatial symmetries for their protection and thus constitute an extension of the notion of topological crystalline phases of matter.

8.4.1 2D model with corner modes

A natural avenue of constructing a higher-order topological phase in 2D is to consider a 2D generalization of the SSH model with unit cell as shown in Fig. 8.3***a*** (disregarding the colors in this figure for now) and alternating hoppings t and t' in both the x and y-directions. However, naively the bulk of the model defined this way with all hoppings of positive sign is gapless. This can be most easily seen in the fully atomic limit $t' = 0$, $t \neq 0$, where the Hamiltonian reduces to a sum over intra-unit cell Hamiltonians of the form

$$\mathcal{H} = t \begin{pmatrix} 0 & 1 & 0 & 1 \\ 1 & 0 & 1 & 0 \\ 0 & 1 & 0 & 1 \\ 1 & 0 & 1 & 0 \end{pmatrix}, \tag{8.4.1}$$

which has obviously zero determinant and therefore gapless modes.
This was amended in a model introduced by Benalcazar, Bernevig and Hughes, which gave the first example of a higher-order topological insulator, by introducing a magnetic flux of π per plaquette. A specific gauge choice realizing this corresponds to reversing the sign of the hoppings along the blue lines in Fig. 8.3***a***. The model then has a gapped bulk, but gapless corner modes. This can be most easily seen in the fully dimerized limit $t = 0$, $t' \neq 0$, where one site in each corner unit cell is not acted upon by any term in the Hamiltonian. However, to protect the corner modes we have to include a spatial symmetry in addition to chiral symmetry, since we could otherwise perform an edge manipulation which leaves the bulk (and in particular, its gap) invariant but annihilates one corner mode with another. A natural candidate for this is the pair of diagonal mirror symmetries M_{xy} and $M_{x\bar{y}}$, which each leave a pair of corners invariant and therefore allow for protected gapless modes on them.
Note that we cannot arrive at the same phase by just combining two one-dimensional SSH models glued to the edges of a trivially gapped 2D system: By the mirror symmetry, the two SSH chains on edges that meet in a corner would have to be in the same topological phase. Thus, each would contribute one corner mode. At a single corner, we would therefore have a pair of modes which is not prevented by symmetry from being shifted to finite energies by a perturbation term. This consideration establishes the bulk model we introduced as an intrinsically 2D topological phase of matter. We will now present three alternative approaches to characterize the topology as well as the gapless corner modes of the model.

Elementary mirror subspace analysis

The plaquettes along the $x\bar{y}$ diagonal are the only parts of the Hamiltonian mapped onto themselves by the $M_{x\bar{y}}$ mirror symmetry. In the fully dimerized limit $t' \neq 0$, $t = 0$, we may consider the Hamiltonian as well as the action of $M_{x\bar{y}}$ on a single inter-unit cell plaquette on the diagonal of the system as given by

$$\mathcal{H} = t' \begin{pmatrix} 0 & 1 & 0 & -1 \\ 1 & 0 & 1 & 0 \\ 0 & 1 & 0 & 1 \\ -1 & 0 & 1 & 0 \end{pmatrix}, \quad M_{x\bar{y}} = \begin{pmatrix} 0 & 0 & 1 & 0 \\ 0 & 1 & 0 & 0 \\ 1 & 0 & 0 & 0 \\ 0 & 0 & 0 & -1 \end{pmatrix}. \tag{8.4.2}$$

$M_{x\bar{y}}$ has eigenvectors

$$|+_1\rangle = \begin{pmatrix} 0 \\ 1 \\ 0 \\ 0 \end{pmatrix}, \quad |+_2\rangle = \frac{1}{\sqrt{2}} \begin{pmatrix} 1 \\ 0 \\ 1 \\ 0 \end{pmatrix}, \quad |-_1\rangle = \begin{pmatrix} 0 \\ 0 \\ 0 \\ 1 \end{pmatrix}, \quad |-_2\rangle = \frac{1}{\sqrt{2}} \begin{pmatrix} 1 \\ 0 \\ -1 \\ 0 \end{pmatrix} \tag{8.4.3}$$

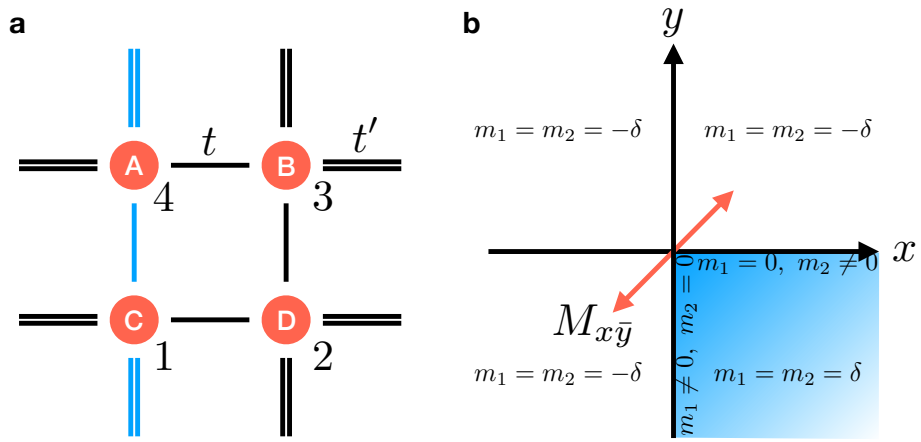

Figure 8.3: Higher-order 2D SSH model. ***a*** The model features intra-unit cell hopping with strength t as well as inter-unit cell hopping with strength t'. For the topological phase we require $t' > t$. In particular, in the fully dimerized limit $t = 0$, $t' \neq 0$ it becomes evident that when we cut the system in two directions to create a corner, there is one dangling site which is not acted upon by any term in the Hamiltonian and therefore provides a zero-mode. The unit cell contains a π-flux per plaquette, which is realized by all blue hoppings being negative, while all black hoppings are positive. ***b*** Vortex geometry of the prefactors of the two masses in Eq. (8.4.9). We imply a smooth interpolation between the mass values given in the bulk, on the edges, and on the outside. At the corner, the masses vanish and they hence form a vortex-like structure around it.

with eigenvalues $+1, +1, -1, -1$, respectively. Since $[\mathcal{H}, M_{x\bar{y}}] = 0$ we know that the Hamiltonian block-diagonalizes into the two mirror subspaces, and we may calculate its form in each Block separately,

$$(\mathcal{H}_+)_{ij} = \langle +_i | \mathcal{H} | +_j \rangle \to \mathcal{H}_+ = \begin{pmatrix} 0 & \sqrt{2} \\ \sqrt{2} & 0 \end{pmatrix} = \mathcal{H}_-. \tag{8.4.4}$$

This, however, is exactly the form taken by a single SSH model in the fully dimerized, and therefore topologically nontrivial, phase (this is because here we have focussed on a plaquette on the diagonal with t' hopping, an adjoining plaquette with t hopping would correspond to the weak bonds in the mirror subspace SSH model). We may therefore interpret our model along one diagonal as two nontrivial SSH models, one for each mirror subspace and protected by the chiral symmetry. Naively this would imply two end modes. However, this is not the case. In the upper left corner, for example, only a single A site is left from an inter-unit cell plaquette (see Fig. 8.3***a***), which happens to have mirror eigenvalue -1. Correspondingly, the lower right corner hosts a dangling D site, which has mirror eigenvalue $+1$. Thus, due to this modified bulk-boundary correspondence of the higher-order topological insulator, each of the two diagonal SSH chains has only one end state at opposite ends. These form the corner modes of the higher-order topological insulator.

Mirror-graded winding number

In analogy to the mirror graded Wilson loop introduced in Sec. 8.1, we can calculate the mirror-graded winding number suited for systems with chiral symmetry. For this we need the full Bloch Hamiltonian, which is given by

$$\mathcal{H}(\boldsymbol{k}) = (1 + \lambda \cos k_x)\tau_0\sigma_x + (1 + \lambda \cos k_y)\tau_y\sigma_y - \lambda \sin k_x \tau_z\sigma_y + \lambda \sin k_y \tau_x\sigma_y. \tag{8.4.5}$$

Note that by a term such as $\sigma_x\tau_0$ we really mean the tensor product $\sigma_x \otimes \tau_0$ of two Pauli matrices. Here, we have chosen $t = 1$ and $t' = \lambda$. The case where $\lambda > 1$ then corresponds to the topological phase. Along the diagonals of the BZ (and only there), the Hamiltonian may again be block-diagonalized by the mirror symmetries. Let us consider for concreteness the $\boldsymbol{k} = (k, k)$ diagonal, which is invariant under M_{xy} with representation

$$M_{xy} = \begin{pmatrix} -1 & 0 & 0 & 0 \\ 0 & 0 & 0 & 1 \\ 0 & 0 & 1 & 0 \\ 0 & 1 & 0 & 0 \end{pmatrix}. \tag{8.4.6}$$

With a transformation that diagonalizes M_{xy}, we can bring the Hamiltonian in the form

$$\tilde{\mathcal{H}}(k,k) = \begin{pmatrix} 0 & q_+(k) & 0 & 0 \\ q_+^\dagger(k) & 0 & 0 & 0 \\ 0 & 0 & 0 & q_-(k) \\ 0 & 0 & q_-^\dagger(k) & 0 \end{pmatrix}, \quad q_\pm(k) = \sqrt{2}(1 + \lambda e^{\mp \mathrm{i}k}). \tag{8.4.7}$$

We see that in the two mirror eigenspaces $\tilde{\mathcal{H}}(k,k)$ takes the form of an SSH model. Defining

$$\nu_\pm = \frac{\mathrm{i}}{2\pi} \int \mathrm{d}k \, \mathrm{Tr}\left[\tilde{q}_\pm(k)\partial_k \tilde{q}_\pm^\dagger(k)\right] \tag{8.4.8}$$

in analogy to our definition of the one-dimensional winding number, where we have appropriately normalized $\tilde{q}_\pm(k) = q_\pm(k)/|q_\pm(k)|$, we obtain $\nu_\pm = \pm 1$ and therefore $\nu_{M_{xy}} = 1$ for the mirror-graded winding number $\nu_{M_{xy}} = (\nu_+ - \nu_-)/2$. As long as the system obeys the mirror symmetry and the chiral symmetry, $\nu_{M_{xy}}$ is a well-defined topological invariant that cannot be changed without closing the bulk gap of the 2D system.

Dirac picture of corner states

An alternative and very fruitful viewpoint of topological phases of matter arises from the study of continuum Dirac Hamiltonians corresponding to a given phase. For example, the band inversion of a first-order topological insulator can be efficiently captured by the Hamiltonian of a single gapped Dirac cone with mass m in the bulk of the material, and mass $(-m)$ in its exterior. One can then show that the domain wall in m binds exactly one gapless Dirac cone to the surface of the material. We want to develop an analogous understanding of higher-order topological phases as exemplified by the model studied in this section.
For the topological phase transition at $\lambda = 1$ in Eq. (8.4.5), there is a gap closing at $\boldsymbol{k}_0 = (\pi, \pi)$. Expanding $\mathcal{H}(\boldsymbol{k})$ around this point to first order and setting $\boldsymbol{k} = \boldsymbol{k}_0 + \boldsymbol{p}$, we obtain

$$\begin{aligned} \mathcal{H}(\boldsymbol{k}) &= (1-\lambda)\tau_0\sigma_x + (1-\lambda)\tau_y\sigma_y + \lambda p_x \, \tau_z\sigma_y - \lambda p_y \, \tau_x\sigma_y \\ &\approx \delta\tau_0\sigma_x + \delta\tau_y\sigma_y + p_x \, \tau_z\sigma_y - p_y \, \tau_x\sigma_y, \end{aligned} \tag{8.4.9}$$

where we have defined $\delta = (1 - \lambda) \ll 1$ and $\lambda \approx 1$. Note that all matrices anticommute and that there are two mass terms, both proportional to δ, in accordance with the gap-closing phase transition at $\delta = 0$. When terminating the system, a boundary is modeled by a spatial dependence of these masses. We consider the geometry shown in Fig. 8.3***b***, where two edges meet in a corner. The mirror symmetry $M_{x\bar{y}}$ maps one edge to the other but leaves the corner invariant. As a result, the mirror symmetry does not pose any restrictions on the masses on one edge, but once their form is determined on one edge, they are also fixed on the other edge by $M_{x\bar{y}}$. In fact, since $M_{x\bar{y}}\tau_0\sigma_x M_{x\bar{y}}^{-1} = \tau_y\sigma_y$ with $M_{x\bar{y}} = (\tau_x\sigma_0 + \tau_z\sigma_0 + \tau_x\sigma_z - \tau_z\sigma_z)/2$ and vice versa, we may consider the particularly convenient choice of Fig. 8.3***b*** for the mass configuration of the corner geometry.

From Fig. 8.3***b***, it becomes evident that the symmetries dictate that the masses, when considered as real and imaginary part of a complex number, wind once around the origin of the corresponding complex plane (at which the system becomes gapless) as we go once around the corner in real space. They are mathematically equivalent to a vortex in a p-wave superconductor, which is known to bind a single Majorana zero-mode. We can therefore infer the presence of a single gapless corner state for the model considered in this section from its Dirac Hamiltonian.
To be more explicit, denoting by $m_1(x,y)$ and $m_2(x,y)$ the position-dependent prefactors of $\sigma_x\tau_0$ and $\sigma_y\tau_y$, respectively, we may adiabatically evolve the Hamiltonian to a form where the mass term vortex is realized in the particularly natural form $m_1(x,y)+\mathrm{i}m_2(x,y) = x+\mathrm{i}y = z$, where z denotes the complex number corresponding to the 2D real space position (x,y). After performing a C_3 rotation about the (111)-axis in τ space, which effects the replacement $\tau_x \to \tau_y \to \tau_z \to \tau_x$, and exchanging the order of τ and σ in the tensor product, the resulting matrix takes on the particularly nice form

$$\begin{aligned} \mathcal{H}(\boldsymbol{k}) &= \begin{pmatrix} 0 & q(\boldsymbol{k}) \\ q^\dagger(\boldsymbol{k}) & 0 \end{pmatrix}, \\ q(\boldsymbol{k}) &= \begin{pmatrix} m_1 - \mathrm{i}m_2 & -\mathrm{i}p_x + p_y \\ -\mathrm{i}p_x - p_y & m_1 + \mathrm{i}m_2 \end{pmatrix} = \begin{pmatrix} \bar{z} & -\partial_{\bar{z}} \\ -\partial_z & z \end{pmatrix} \\ \to \quad q^\dagger(\boldsymbol{k}) &= \begin{pmatrix} z & \partial_{\bar{z}} \\ \partial_z & \bar{z} \end{pmatrix}. \end{aligned} \tag{8.4.10}$$

While for $q^\dagger(\boldsymbol{k})$, there is one zero-energy solution $|\Psi\rangle = e^{-z\bar{z}}(1,1)$, the corresponding solution $|\tilde{\Psi}\rangle = e^{\frac{z^2+\bar{z}^2}{2}}(1,1)$ for $q(\boldsymbol{k})$ is not normalizable. We thus conclude that there is one zero-mode with eigenfunction $(|\Psi\rangle, |0\rangle)$ localized at the corner of the sample.

8.4.2 3D model with hinge modes

To construct a higher-order topological insulator in 3D, we start from a time-reversal invariant topological crystalline insulator with mirror Chern numbers in its bulk BZ. For the sake of simplicity we restrict to the case where only the mirror Chern number C_m belonging to the M_y symmetry is non-vanishing because the argument goes through for each mirror Chern number separately. We will now show that in an open geometry with surface normals along the xy and $x\bar{y}$ direction, $C_\mathrm{m} = 2$ implies the presence of a single time-reversal pair of gapless chiral hinge modes on the intersection of the (110) and $(1\bar{1}0)$ surfaces (see Fig. 8.4).
As discussed in Sec. 8.2, for M_y symmetry, a nonzero $C_\mathrm{m} = 2$ enforces two gapless Dirac cones in the surface BZ of the (100) termination, which is mapped onto itself by M_y. Note that on this surface, with normal in x-direction, k_y and k_z are still good momentum quantum numbers. The Hamiltonian for a single surface Dirac cone can be written as

$$\mathcal{H}(k_y, k_z) = v_1\sigma_z k_y + v_z\sigma_x(k_z - k_z^0), \tag{8.4.11}$$

where the mirror symmetry is represented by $M_y = \mathrm{i}\sigma_x$ and thus prevents a mass term of the form $+m\sigma_y$ from appearing. To arrive at a theory describing the intersection of the (110) and $(1\bar{1}0)$ boundaries, we introduce a mirror-symmetric kink in the (100) surface (see Fig. 8.4***a***) and so first consider the intersection of two perturbatively small rotations of the (100) surface, one to a $(1,\alpha,0)$ termination and the other to a $(1,-\alpha,0)$ termination with $\alpha \ll 1$. The Hamiltonian on the $(1,\pm\alpha,0)$ surface becomes

$$\begin{aligned} \mathcal{H}_\pm(k_y, k_z) &= v_1\sigma_z(k_y \pm \rho) + v_z\sigma_x(k_z - k_z^0) \pm m\sigma_y \\ &\equiv v_1\tilde{k}_y^\pm\sigma_z + v_z\tilde{k}_z\sigma_x \pm m\sigma_y, \end{aligned} \tag{8.4.12}$$

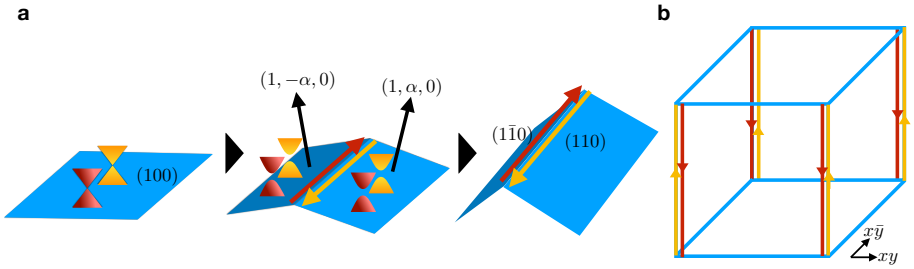

Figure 8.4: Construction of a 3D second-order topological insulator. ***a*** We begin with a surface left invariant by M_y on which $C_\mathrm{m} = 2$ implies two gapless Dirac cones. When slightly tilting the surface in opposite directions to form a kink, the Dirac cones on the new surfaces on either side of the kink may be gapped out with opposite masses, since the mirror symmetry maps one into the other and anti commutes with the Dirac mass term. Since a domain wall in a Dirac mass binds a single zero-mode, and the two Dirac cones on each surface are mapped into each other by time-reversal, a Kramers pair of gapless hinge modes emerges on the intersection. When continuing to bend the surfaces to create a right angle, these modes cannot vanish since they are protected by the M_y mirror symmetry. ***b*** By this argument we can infer time-reversal paired hinge modes on each hinge along the x (and y, if we also take into account the mirror symmetry M_x along with $C_\mathrm{m} = 2$) direction.

where m and ρ are small parameters of order α and we have omitted the irrelevant coordinate shifts in the last line. This Hamiltonian describes a gapped Dirac cone, the mass term is now allowed by mirror symmetry since the surfaces considered are no longer invariant under it. Instead, they are mapped onto each other and thus have to carry opposite mass. We note that by this consideration the hinge between the $(1,\alpha,0)$ and $(1,-\alpha,0)$ surfaces constitutes a domain wall in a Dirac mass extended in z-direction, which is known to host a single chiral mode.
We will now explicitly solve for this domain wall mode at $\tilde{k}_z = 0$ by going to real space in y-direction. Making the replacement $\tilde{k}_y^{\pm} \to -\mathrm{i}\partial_y$, the Hamiltonian on either side of the hinge becomes

$$\mathcal{H}_\pm = \begin{pmatrix} -\mathrm{i}v_1\partial_y & \pm \mathrm{i}m \\ \mp \mathrm{i}m & \mathrm{i}v_1\partial_y \end{pmatrix}. \tag{8.4.13}$$

$\mathcal{H}_+$, for which $y > 0$, has one normalizable zero-energy solution given by $|\Psi_+\rangle = e^{-\kappa y}(1,1)$ (where we assume $\kappa = m/v_1 > 0$ without loss of generality). $\mathcal{H}_-$, for which $y < 0$, has another normalizable zero-energy solution given by $|\Psi_-\rangle = e^{\kappa y}(1,1)$. Since the spinor $(1,1)$ of the solutions is the same on either side of the hinge, the two solutions can be matched up in a continuous wave function. We obtain a single normalizable zero-energy solution for the full system at $k_z = 0$, which is falling off exponentially away from the hinge with a real-space dependence given by $|\Psi\rangle = e^{-\kappa|y|}(1,1)$. To determine its dispersion, we may calculate the energy shift for an infinitesimal k_z in first-order perturbation theory to find

$$\Delta E(\tilde{k}_z) = \langle\Psi|\, v_z\tilde{k}_z\sigma_x\, |\Psi\rangle = +v_z\tilde{k}_z \tag{8.4.14}$$

We have therefore established the presence of a single linearly dispersing chiral mode on the hinge between the $(1,\alpha,0)$ and $(1,-\alpha,0)$ surfaces by considering what happens to a single Dirac cone on the $(1,0,0)$ surface when a kink is introduced. The full model, which by $C_\mathrm{m} = 2$ has two (100) surface Dirac cones paired by time-reversal symmetry, therefore hosts a Kramers pair of hinge modes on the intersection between the $(1,\alpha,0)$ and $(1,-\alpha,0)$ surfaces. These surfaces themselves are gapped. The two modes forming the hinge Kramers pair have opposite mirror eigenvalue. Increasing α non-perturbatively to 1 in a mirror-symmetric fashion cannot change the number of these hinge modes, since the chiral modes belong to different mirror subspaces

and are thus stable to any perturbation preserving the mirror symmetry. By this reasoning, we end up with a pair of chiral modes at each hinge in the geometry of Fig. 8.4***b***.